Quantitative Collection and Enzymatic Activity of Glucose Oxidase Nanotubes Fabricated by Templated Layer-by-Layer Assembly

ARTICLE *in* BIOMACROMOLECULES · JULY 2015

Impact Factor: 5.75 · DOI: 10.1021/acs.biomac.5b00628 · Source: PubMed

3 AUTHORS:

Shouwei Zhang

Université catholique de Louvain

4 PUBLICATIONS **4** CITATIONS

SEE PROFILE

Sophie Demoustier-Champagne

Université catholique de Louvain

125 PUBLICATIONS **3,046** CITATIONS

SEE PROFILE

Alain M. Jonas

Université catholique de Louvain

260 PUBLICATIONS **5,392** CITATIONS

SEE PROFILE

Article

pubs.acs.org/Biomac

Quantitative Collection and Enzymatic Activity of Glucose Oxidase Nanotubes Fabricated by Templated Layer-by-Layer Assembly

Shouwei Zhang, Sophie Demoustier-Champagne,* and Alain M. Jonas*

Institute of Condensed Matter and Nanosciences - Bio and Soft Matter (IMCN/BSMA), Université Catholique de Louvain, Croix du Sud 1/L7.04.02, B1348 Louvain-la-Neuve, Belgium

Supporting Information

ABSTRACT: We report on the fabrication of enzyme nanotubes in nanoporous polycarbonate membranes via the layer-by-layer (LbL) alternate assembly of polyethylenimine (PEI) and glucose oxidase (GOX), followed by dissolution of the sacrificial template in CH_2Cl_2, collection, and final dispersion in water. An adjuvant-assisted filtration methodology is exploited to extract quantitatively the nanotubes without loss of activity and morphology. Different water-soluble CH_2Cl_2-insoluble adjuvants are tested for maximal enzyme activity and nanotube stability; whereas NaCl disrupts the tubes by screening electrostatic interactions, the high osmotic pressure created by fructose also contributes to loosening the nanotubular structures. These issues are solved when using neutral, high molar mass dextran. The enzymatic activity of intact free nanotubes in water is then quantitatively compared to membrane-embedded nanotubes, showing that the liberated nanotubes have a higher catalytic activity in proportion to their larger exposed surface. Our study thus discloses a robust and general methodology for the fabrication and quantitative collection of enzymatic nanotubes and shows that LbL assembly provides access to efficient enzyme carriers for use as catalytic swarming agents.

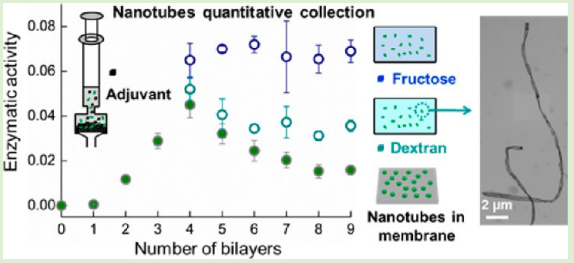

INTRODUCTION

In natural biochemical processes, enzymatic reactions often occur in the spatially confined environment of extremely small compartments, resulting in an improved specificity and activity.[1] This inspired the synthesis of artificial nanostructures for performing reactions in confinement; different morphologies were developed, varying from spherical to tubular, such as nanoporous organic crystalline hosts,[2] micelles and vesicles, or nanocapsules[3−10] and nanotubes,[11−15] enabling confinement effects to be experimentally studied with these synthetic analogues.

Among different possible building components,[16−19] biomacromolecules are especially interesting for inclusion in such biomimetic nanostructures. In particular, protein-based nanotubes, which present several advantages over nanospheres,[20] are attracting an increasing interest because of their potential applications in various fields, for instance as drug nanocarriers,[21] as enzyme-powered micromotors for water-quality testing,[11] as biochannels[13] or bioreactors,[14] or as bioanodes for biofuel cells.[22] Compared to free enzymes, nanotubes may offer a protective shell to stabilize enzymes and may substantially ease the recovery of enzymes after use. Thanks to the mild adsorption conditions of layer-by-layer (LbL) assembly,[23] protein-based tubular nanocylinders have been recently achieved via the assembly of two different oppositely charged proteins and counter-polyelectrolytes[24−31] in nanoporous membranes, such as anodic aluminum oxide (AAO) or track-etched polycarbonate (PC) membranes. After dissolution of the membrane template, nanotubes are obtained, somehow reminiscent of natural protein cages or viral capsids.[32] Among these protein-containing LbL nanotubes, enzyme-based nanotubes are expected to be promising artificial agents for biocatalysis.

However, few reports focus on the morphology and properties of nanotubes composed of natural enzymes liberated from their templating membrane. Martin et al.[15] first reported on the fabrication of glucose oxidase (GOX) nanotubes in porous AAO templates with an interlayer cross-linker, glutaraldehyde. Although the liberated nanotubes retained the enzymatic activity of immobilized GOX, most of them were broken during the template dissolution process due to the harsh conditions required for the removal of AAO (phosphoric acid solution). The soft extraction of nanotubes from the template framework is indeed still a challenge for template-assisted synthesis.[33] As for nanoporous polymer membranes, which can be more easily dissolved in organic solvents, the difficulty is to separate the nanotubes from the dissolved polymer solution.

Recently, Komatsu et al.[14] proposed an effective approach to collect enzymatic LbL nanotubes containing human serum albumin (HSA), released from a PC polymer membrane. After the nanotubes were liberated by dissolution in *N*,*N*-dimethylformamide (DMF), they were precipitated from the resultant polymer solution and washed with fresh DMF by

Received: May 11, 2015
Revised: July 1, 2015

DOI: 10.1021/acs.biomac.5b00628
Biomacromolecules XXXX, XXX, XXX−XXX

Scheme 1. Schematic Illustration of the Fabrication of Free Enzyme Nanotubes in a Nanoporous PC Membrane

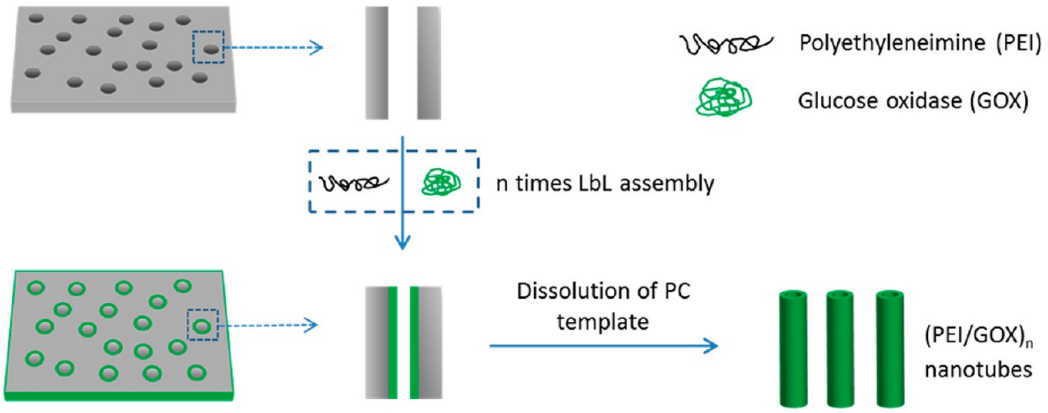

centrifugation. The nanotubes were then rapidly freeze-dried to produce a lyophilized powder that could readily be dispersed in deionized water. This process allowed the enzyme-modified nanotubes not only to retain their tubular structures but also to preserve their activity in an aqueous environment. Here, we develop an alternative collection methodology of LbL-templated enzymatic nanotubes containing glucose oxidase (GOX), which allows us to recover quantitatively sticky soft nanotubes in gentle conditions without degradation, thus, permitting for the first time a quantitative comparison of the activity of membrane-embedded and released enzymatic nanotubes.

Owing to the complexity of protein structure and the patchy nature of their distribution of surface charge, the assembly of proteins with oppositely charged polyelectrolytes is not always possible.[13,34,35] For instance, it was reported that only branched polyethylenimine (bPEI) or poly-L-arginine (PLA) could be combined with HSA to produce stable nanotubes by LbL deposition in PC templates.[26] Likewise, we failed to build stable GOX nanotubes when paired with chitosan because the addition of chitosan desorbed heavily the previously adsorbed GOX as was checked by ellipsometry on flat multilayers. Therefore, bPEI is used here as the electrostatic glue for LbL assembly with GOX. The assembly conditions such as nature, concentration, and pH of the deposition buffer are optimized, aiming at producing robust enzyme nanotubes of high enzymatic activity. After the enzyme nanotubes are successfully collected from templates by our new methodology, the activity of liberated nanotubes in aqueous dispersion is examined and compared to the one of the nanotubes still embedded in the PC membrane.

EXPERIMENTAL SECTION

Materials. Glucose oxidase (GOX, 160 kDa, type x-s lyophilized powder, 100000−250000 units/g), horseradish peroxidase (HRP, Type VI, lyophilized powder, 250−330 units/mg solid), branched polyethylenimine (bPEI, M_n ca. 60000, M_w ca. 750000 g·mol^{-1}), *o*-dianisidinedihydrochloride, 4-morpholineethanesulfonic acid (MES), glucose, fructose, and dextran (M_r ∼ 70000, Leuconostoc spp.) were purchased from Sigma-Aldrich. Linear polyethylenimine (lPEI, Mw = 100,000 g·mol^{-1}) and chitosan (CHI, DDA > 90%, Mw ca. 270,000 g·mol^{-1}) were obtained from Polysciences and Novamatrix, respectively. 2-[4-(2-Hydroxyethyl)-1-piperazine] ethanesulfonic acid (HEPES free acid), potassium bromide (FT-IR grade, ≥ 99%), and dichloromethane (99.8%, for analysis) were from Acros Organics. All polyelectrolyte and GOX solutions were freshly prepared at a concentration of 1.0 mg/mL either in water (pH 6.5) or in buffer (pH 6.5−8.0, 10 mM or 25 mM HEPES buffer and 10 mM MES buffer). In these conditions, GOX has a negative charge given an isoelectric point of 4.2,[35−37] and PEI is positively charged.[38,39] Milli-Q water with 18.2 MΩ·cm resistivity was used in all experiments. Track-etched polycarbonate (PC) membranes (Figure S1A) of 300 nm average pore diameter, 25 μm thickness, and 1 × 10^8 cm^{-2} pore density were used as templates for LbL deposition, whereas poly(ethylene terephthalate) (PET) membranes of 200 nm average pore size, 23 μm thickness, and 5 × 10^8 cm^{-2} pore density were used as filters; both types of membranes were provided by the it4ip company, Louvain-la-Neuve, Belgium (http://www.it4ip.be).

Templated Synthesis of PEI/GOX Nanotubes. The enzyme-containing nanotubes were fabricated according to the procedure shown in Scheme 1. Briefly, a piece of PC membrane was first dipped in a PEI solution, immediately sonicated for 15 min to ease transportation of PEI into the pores, then allowed 30 min for adsorption; this was followed by two rinses of 3 min each in the same but polyelectrolyte-free aqueous solution as used for adsorption. The PEI-modified porous PC membrane was then immersed in the GOX solution, following the same protocol as used for adsorbing the PEI layer. After each GOX deposition, the polyelectrolyte crust deposited on the top and bottom surfaces of the membrane was removed with a cotton swab. All depositions were performed manually at ambient temperature. No drying step was performed during the whole procedure until the desired number of bilayers was reached. When buffer was used throughout the process, including rinsing, the nanotube-modified membrane was rinsed at the end of entire process in pure water for 1 min to remove the buffer salt, followed by a final decrusting of the top and bottom surfaces with a cotton swab to make sure the surface films were eliminated completely. An identical final decrusting treatment was carried out for the samples with intervening rinses in water. The prepared membranes were stored at 4 °C in the dry state in a fridge and were used within 2 days.

Gas Flow Porometry Measurements. LbL growth on nanopore walls was monitored by measuring the evolution of the average pore diameter with the number of deposited bilayers. This was performed using gas flow porometry at room temperature on air-dried samples. For each sample, three different spots were measured. Prior to measurements on samples, tests on the virgin membrane were conducted, and the flow value was used as reference for normalization, assuming a pore diameter of about 300 nm (as measured by SEM). The measured pore diameter for each sample was an average of at least 9 measurements. Details regarding the setup and analysis were reported in a previous publication.[40]

Collection of Enzyme Nanotubes. The PC membrane was dissolved in CH_2Cl_2 to release the nanotubes, which were collected by filtration over a PET nanoporous membrane. Preliminary experiments showed that the nanotubes could never be released in water from the filter, once having been in contact with the virgin PET filter. Therefore, free nanotubes were recovered by a filtration method involving water-soluble powder (salt, fructose or dextran) as filtration adjuvant, as shown in Scheme 2. A finely crushed powder was first

DOI: 10.1021/acs.biomac.5b00628
Biomacromolecules XXXX, XXX, XXX−XXX

Scheme 2. Collection of Enzyme Nanotubes by Powder-Assisted Filtration: (A) Resultant Cake with Nanotubes, (B) Au Covered PET Filter after Filtration and Removal of the Cake, (C) Aqueous Suspension of Free Nanotubes Obtained by Dissolving the Whole Cake

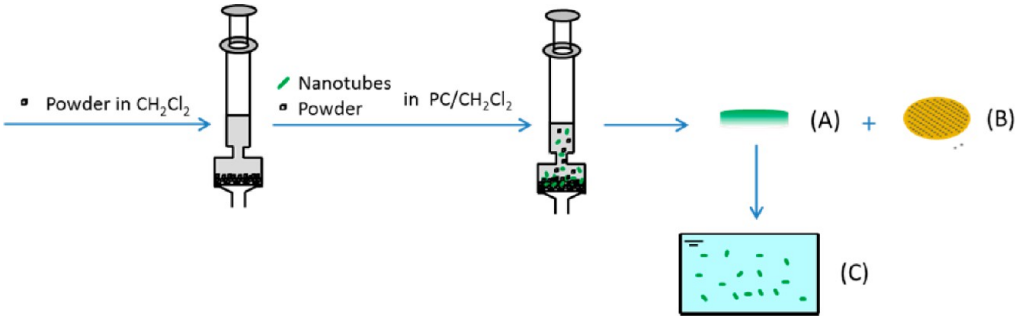

suspended in CH_2Cl_2 and filtered on a nanoporous PET membrane clamped in a stainless steel syringe holder (13 mm diameter, Millipore Corp.). This resulted in the formation of a thin powdery cake on the filter, which subsequently served as a leaky barrier layer, preventing the nanotubes from reaching the PET membrane. Then, the same powdered adjuvant was added to the nanotube suspension in PC/CH_2Cl_2, and the resulting suspension was filtered over the previous cake and rinsed three times with fresh CH_2Cl_2 for complete elimination of the dissolved PC. At the end of the process, the cake containing the nanotubes adsorbed on the adjuvant was easily detached from the PET filter; immersion in water dissolved the cake, leading to a clear aqueous suspension of liberated nanotubes.

SEM and STEM Characterization of Enzyme Nanotubes. The morphology of the enzyme nanotubes was evaluated with a field emission scanning electron microscope (JSM-7600F, JEOL Ltd.), equipped with a transmission detector, operated at 15 and 30 kV for the scanning mode (SEM) and for the scanning transmission mode (STEM), respectively. To observe the nanotubes collected from PC/CH_2Cl_2, the samples for SEM were prepared by filtration of the nanotube suspension in PC/CH_2Cl_2 through PET membranes covered by 20 nm of gold (Cressington Sputter Coater 208HR), and then rinsed several times by pure CH_2Cl_2 before observation; for STEM, carbon-coated copper grids (200 mesh, Electron Microscopy Sciences) were placed in the nanotube suspension and agitated gently for 1 min, then washed by CH_2Cl_2, and air-dried at room temperature. In another approach to prepare samples for STEM observation (Scheme S1, Supporting Information), the filled PC template was floated over a thin layer of water cast on a Si wafer, left to impregnate for 30 min, then placed at −20 °C until water crystallized. Subsequent dissolution by CH_2Cl_2 of the PC membrane (three immersions in cold CH_2Cl_2 below 0 °C), followed by ice melting, yielded a thin film of nanotubes floating over water, which was transferred to a carbon-coated copper grid and dried. For the observation of liberated nanotubes in aqueous solution, the samples for SEM were collected either by filtration of an aqueous suspension of nanotubes through an Au/Cr-coated PET membrane or by dipping an Au/Cr-coated PET membrane in the nanotube suspension (2 mL). Likewise for STEM, a carbon-coated grid was immersed in the aqueous suspension of nanotubes.

FTIR Measurements and Analysis. Fourier transform infrared (FTIR) spectra were collected at 8 cm^{-1} resolution (128 passes) on a FTIR spectrometer (Nicolet Nexus 870, Thermo Scientific). For nanotubes, the samples were prepared by filtration on a PET membrane as follows. A fine KBr powder suspended in CH_2Cl_2 was first filtered on the nanoporous PET membrane. Then the nanotube suspension in PC/CH_2Cl_2 was filtered gently to separate the PC from the nanotubes. The KBr powder with entrapped nanotubes was collected after rinsing with pure CH_2Cl_2 and drying at 60 °C for 1 day and used to prepare a KBr disk containing nanotubes for FTIR. For free glucose oxidase, polyethylenimine and their mixtures, a standard KBr disk was prepared, except when the product was a liquid, in which case it was simply deposited over an IR-transparent support (ZnSe crystal).

For the quantitative analysis of bPEI/GOX nanotubes, the raw spectra of pure bPEI and GOX were first recorded and used to fit the spectra of a series of mixtures of bPEI and GOX prepared with a known ratio by weight, according to

$$A_{\text{mixture}} = F_{\text{bPEI}}A_{\text{bPEI}} + F_{\text{GOX}}A_{\text{GOX}} + F_{\text{KBr}}A_{\text{KBr}} + a + bk + ck^2 + dk^3$$

where A_{mixture}, A_{GOX}, A_{bPEI}, and A_{KBr} are the absorbances of the mixture, pure bPEI, GOX, and KBr, respectively, F_{GOX}, F_{bPEI}, and F_{KBr} are the corresponding scale factors, and the polynomial expression of third order in the wavenumber k is the baseline. The fit was performed from 1410 to 1780 cm^{-1}, in a region presenting well-separated peaks of the two components, excluding the 1504−1569 cm^{-1} spectral region in which the spectra of the mixtures could not be represented as linear combinations of the spectra of the pure components, probably due to specific interactions (Figure S2). The fit of the mixtures allowed us to draw a calibration curve reporting $F_{\text{bPEI}}/F_{\text{GOX}}$ versus the known weight ratio of the samples, $W_{\text{bPEI}}/W_{\text{GOX}}$ (Table S1, Figure S3). The nanotube spectra were analyzed in the same way, with the spectrum of a pure PC membrane included to take into account traces of improperly washed PC (Figures S4 and S5). The ratio by weight of bPEI to GOX in the nanotubes, computed from the values of $F_{\text{bPEI}}/F_{\text{GOX}}$ obtained by the fit and from the calibration curve, are summarized in Table S2 for all tested samples.

Enzyme Activity. To measure the activity of nanotubes in membranes, disks of 10 mm diameter were cut from the (possibly partially) filled membranes; then, 2.00 mL of a 0.3 mM *o*-dianisidinedihydrochloride solution in 50 mM sodium acetate buffer (pH 5.5) and 0.20 mL of a horseradish peroxidase (HRP) solution (containing approximately 60 units mL^{-1}) were mixed in a cuvette with the nanotube-containing membrane and air-equilibrated. A total of 0.50 mL of a 3.0 mM glucose solution was then added to the mixture, and the increase in absorbance at 460 nm (maximum absorption) was recorded at room temperature every 2 min immediately after mixing for 20 min, during which continuous shaking was applied (KS-15 shaker, Edmund Bühler GmbH). The activity of reference planar LbL films grown on flat silicon squares (11 mm × 11 mm) was measured similarly. The activity of liberated nanotubes was evaluated as follows: The extraction of nanotubes from the PC membrane (disks of 10 mm diameter) was achieved as described above, the only difference being that the obtained powder/nanotube cake was immediately dissolved for some time (depending on the nature of powder) on a shaker in a cell containing a mixture of 2.00 mL of a 0.3 mM *o*-dianisidinedihydrochloride solution in 50 mM sodium acetate buffer (pH 5.5) and 0.20 mL of a HRP solution until the cake was dissolved completely. The solution was collected in a cuvette to measure the absorbance at 460 nm every 1 or 2 min, after addition of 0.50 mL of a 3.0 mM glucose solution. The enzyme activity was defined as the initial rate of the coupled reaction, that is, the initial increase per min of the absorbance at 460 nm, $\Delta A_{460\ \text{nm}}$/min.

DOI: 10.1021/acs.biomac.5b00628
Biomacromolecules XXXX, XXX, XXX−XXX

RESULTS AND DISCUSSION

Selection of the Conditions of LbL Deposition. The growth of LbL films and their internal structure are determined by the nature of polyelectrolytes and the assembly conditions, typically pH, ionic strength of polyelectrolyte solutions, and use or not of intermediate drying steps.[41,42] Herein, the assembly conditions were optimized for alternate deposition of bPEI or lPEI (linear PEI) with GOX into nanoporous PC membranes, varying pH from 6.5 to 8, ionic strength (either 0 or 0.1 M), and rinse with Milli-Q water or buffer (HEPES or MES), aiming at robust enzyme nanotubes of high activity able to survive detemplating. Similar thicknesses of the nanotube walls were obtained within 25% for most tested conditions (Figure 1A), with the LbL growth characterized by a regular diminution of dry pore diameters, demonstrating that the assembly of PEI and GOX occurs well in the nanopores. However, two conditions led to a slower LbL growth, namely, in the presence of 0.1 M NaCl (in bPEI solution), and when using linear PEI (lPEI). This indicates that lower ionic strengths and branches on the PEI facilitate the buildup of enzyme nanotubes, yielding thicker nanotube walls of presumably improved structural stability.

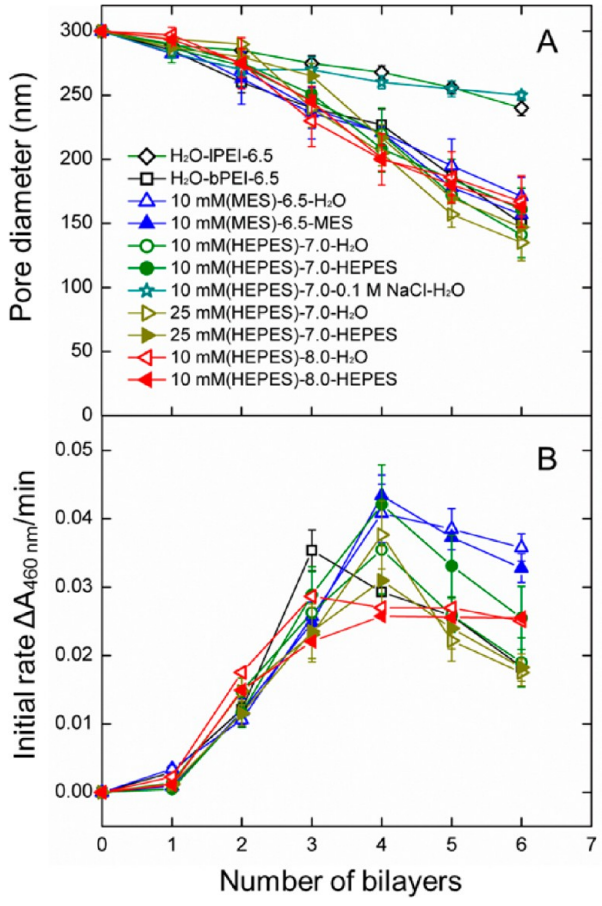

Figure 1. LbL growth of nanotubes in nanopores (of 300 nm initial diameter) determined by measuring the dry pore diameters by gas-flow porometry for different deposition conditions (panel A), and enzymatic activity ($\Delta A_{460\ nm}$/min) of the corresponding membranes with embedded nanotubes (panel B), as a function of the number of deposited bilayers. The sample denomination is (solvent used for the deposition)-(solvent pH)-(solvent used for rinsing), where branched poly(ethylenimine) (bPEI) was used for deposition, except for two samples "H_2O-*x*PEI-6.5", which were fabricated by deposition of either linear (lPEI) or branched (bPEI) poly(ethylenimine) in water (pH = 6.5) and a subsequent rinse in Milli-Q water. The same symbols are used in (B) as in (A).

To eliminate the films covering the surface of the membranes, a decrusting protocol using a cotton swab to clean the membrane was used as reported previously,[26,27,40,43] rather than other harder methodologies such as plasma etching[44] or polishing with alumina powder;[45,46] in our case, however, the cotton swab was saturated with the buffer solution used during the rinsing process. Thereby, the encrusting film on the membrane surfaces could be readily and completely wiped off as revealed by SEM (Figure S1B). In addition, SEM clearly shows the deposition of a LbL layer over the inner walls of the nanopores, although the nanotube lumen fluctuates somewhat from tube to tube (Figure S1B); in contrast, gas-flow porometry provides an average pore diameter (Figure 1A) that probably better represents the average filling of the pores.

With the enzyme film growing on the inner surface of the pores, the enzymatic activity of the nanotube-implanted membranes increased rapidly toward a high value within 3 to 4 bilayers, followed by a decrease or plateau upon additional deposition of enzyme layers (Figure 1B). This is most probably due to a reduced diffusion rate of the glucose substrate in the more filled pores, as already reported before,[15] or in pores having a clogged end, as can be observed in Figure S1a. Hence, the restricted diffusion of the substrate in the filled pores dominates the activity of the partially filled membranes for three or more bilayers as a result of decreased lumen size; it should be reminded here that the pore sizes reported in Figure 1A are average values for systems in the dry state, whereas the activity of the membranes is measured in an aqueous solution that swells the LbL and consequently closes further the pores.[27]

Although a similar LbL growth evolution in nanopores was observed for most tested conditions, significant differences in enzymatic activity are nevertheless observed between the systems. Membranes modified in 10 mM MES buffer (pH 6.5), regardless of the type of rinsing (buffer or pure water), or in 10 mM HEPES (pH 7.0) rinsed in HEPES buffer, have a higher activity (ca. 0.04 min^{-1}) at four bilayers, compared to other preparation conditions. In contrast, the lower activity (ca. 0.026 min^{-1}) is obtained for membranes prepared in 10 mM HEPES (pH 8.0) irrespective of the rinsing process. After four bilayers (or three bilayers only in H_2O at pH 6.5), the activity decreases rapidly except for 10 mM HEPES (pH 8.0) for which the activity only slightly decreases or even keeps constant. These complex effects arise from different enzyme loadings and variations in the ability of the substrate to access the enzyme, which is itself related to the amount and distribution of adsorbed enzyme, residual pore size, and degree of complexation between the enzyme and PEI.

As a rule of thumb, it appears better to keep LbL films at a constant pH during the whole buildup process, using the same medium for intermediate washing steps; indeed, the ionization of adsorbed chains can change upon exposure to media of different pH, inducing the reorganization of previously adsorbed layers, resulting in a film of different properties.[47] From these results, 10 mM MES buffer (pH = 6.5) or 10 mM HEPES (pH = 7.0) buffer appear as most suitable for the construction of GOX-based nanotubes of high activity; hence, these conditions will be taken in the sequel. In addition, only branched PEI will be used in what follows.

DOI: 10.1021/acs.biomac.5b00628
Biomacromolecules XXXX, XXX, XXX−XXX

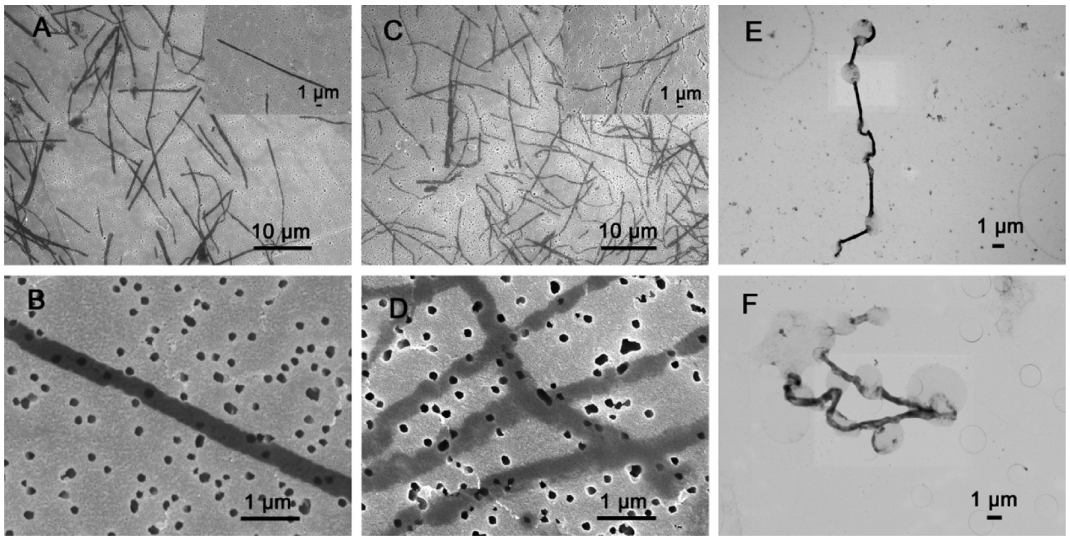

Figure 2. SEM images of $(bPEI/GOX)_6$ nanotubes fabricated in 10 mM HEPES buffer (pH 7.0) throughout (A, B) and 10 mM MES buffer (pH 6.5) throughout (C, D) and corresponding STEM images (E, F). The nanotubes were collected by filtration from CH_2Cl_2 solutions over PET membranes or by adsorption over TEM grids, just after dissolution of the PC membrane.

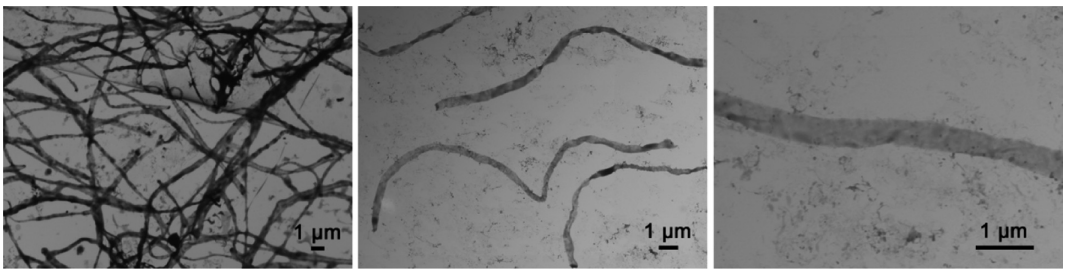

Figure 3. STEM images of free nanotubes fabricated in 10 mM HEPES (pH 7.0) buffer throughout. The nanotubes were extracted after immobilization over an ice layer (Scheme S1), followed by dissolution of the PC template containing frozen nanotubes to avoid the bursting of portions of nanotubes during drying.

Morphology of the Nanotubes. The morphology of nanotubes built in our two optimized conditions was observed by SEM and STEM. Samples for SEM were prepared by collecting the nanotubes by dissolution of the membrane and direct filtration from the resulting suspension in CH_2Cl_2 (Figure 2). Well-defined cylindrical structures were obtained for both preparation conditions; however, nanotubes prepared in 10 mM HEPES buffer (pH 7.0) tend to be more rigid and less deformed. Intact nanotubes of about 25 μm length, well replicating the nanopores, were generally obtained, suggesting that the inner surfaces of the nanopores could be coated all along their length during LbL assembly. Their outer diameter is about 400 nm (Figure 2B,D), moderately larger than the virgin pore size (300 nm), which is due to the flattening of the liberated nanotubes on the filters upon drying. This flattening often makes the observation of the inner cylindrical open channel of the nanotubes difficult. However, STEM allowed in many cases to observe the presence of this open channel (Figure S1b). In addition, individual nanotubes without aggregation were generally observed, confirming the efficient and complete removal of the crust layers on the flat surfaces of the templates.

STEM images (Figure 2E,F) provided comparable information regarding the nanotube morphology. However, the nanotubes appear to have burst at specific locations along their length, which was not seen in SEM images. This phenomenon is due to the capillary forces exerted on the tubes upon CH_2Cl_2 drying, combined with a different interaction strength between the nanotubes on either the PET filter or the carbon-coated TEM grid. To confirm this contention, the specimens for STEM were prepared by another methodology, involving immobilization of the membrane on a layer of ice (Scheme S1), followed by PC dissolution in CH_2Cl_2 with the nanotubes anchored on the ice, leaving a bare nanotube array. With this methodology, intact nanotubes without structural defects could be transferred to a carbon-coated TEM grid (Figure 3), showing that the replacement of CH_2Cl_2 by water in the drying step solved the issue. Unfortunately, the lower temperature also leads to a decreased solubility of PC in CH_2Cl_2, which complicates the complete removal of PC from the tubes; moreover, the liberated nanotubes tend to pack irreversibly in thick bundles when using this methodology (Figure S6).

Based on their more sturdy morphology, nanotubes fabricated in 10 mM HEPES buffer (pH 7.0) throughout were chosen for exploring confined biocatalysis in membrane-supported and liberated nanotubes.

Collection of Free Nanotubes in Water. To achieve our goal of measuring the activity of free nanotubes, these should be extracted from the PC template and dispersed in water, the essential environment where enzymatic reactions occur. This has to be performed with minimal losses, as quantitative

DOI: 10.1021/acs.biomac.5b00628
Biomacromolecules XXXX, XXX, XXX−XXX

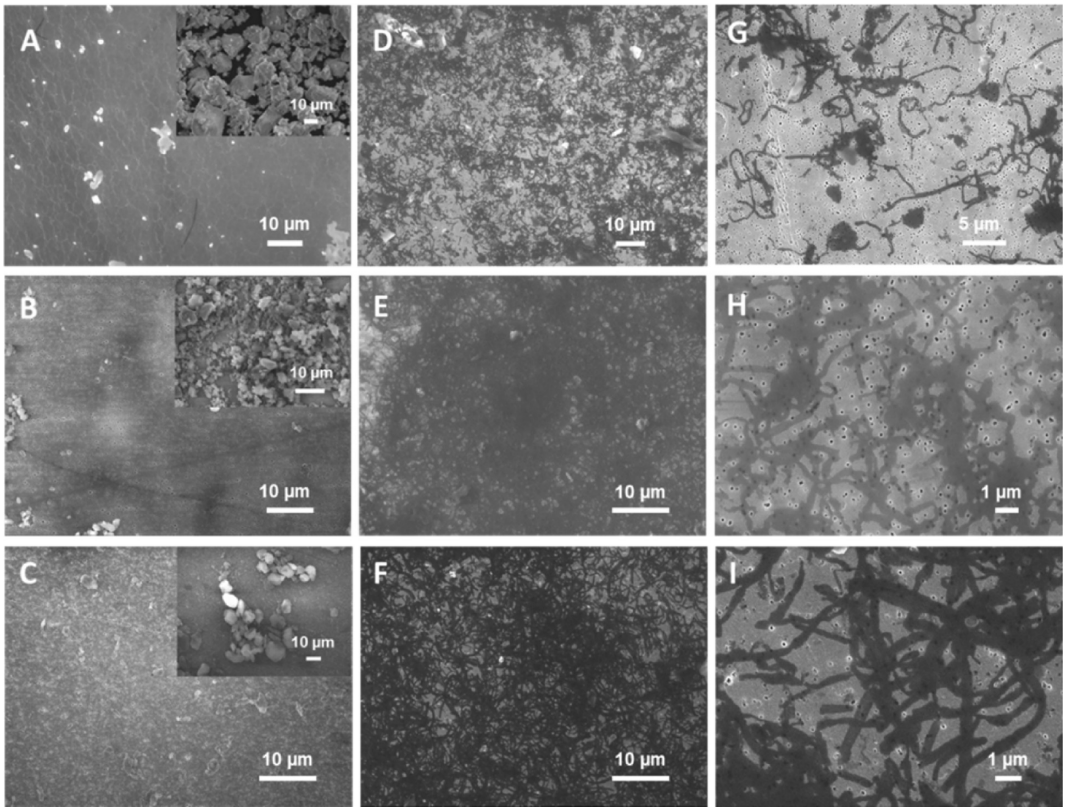

Figure 4. SEM images of the samples obtained by the adjuvant-assisted collection process: (A, D, G) with NaCl as adjuvant; (B, E, H) with fructose as adjuvant; (C, F, I) with dextran as adjuvant. Images (A−C) show the surface of the PET filter after removal of the cake, with almost no residual nanotube on the surface; insets give the morphology of the adjuvant powder. Images (D−I) are nanotubes recovered over an Au/Cr-covered PET membrane by filtration from an aqueous dispersion obtained by dissolving the corresponding adjuvant/nanotube cake in water. When NaCl was used as adjuvant, the nanotubes were collected over the adjuvant cake without adding NaCl adjuvant in the nanotube suspension in the second step of the collection procedure; for other adjuvants, the complete procedure of Scheme 2 was used.

comparisons require to work on a constant number of nanotubes. However, once in contact with the PET filter for recovery after PC dissolution, the nanotubes did not disperse again in water, irreversibly sticking together and to the PET membrane. A modified filtration method was thus developed to collect the nanotubes from the polymer solution, namely adjuvant-assisted filtration (Scheme 2). Sequential filtrations of a dispersion of finely ground adjuvant powder in CH_2Cl_2, then of a suspension of this adjuvant powder added to the nanotubes/dissolved PC in CH_2Cl_2, were carried out on a PET membrane of 200 nm pore size. The adjuvant powder, NaCl, fructose, or dextran, was selected so as to be soluble in water and insoluble in CH_2Cl_2.

The first step of our collection procedure, the filtration of the adjuvant powder, results in the formation of a thin porous cake over the filter, acting as a barrier layer preventing the nanotubes from reaching the PET filter while still allowing filtration. Very few nanotubes can pass through this barrier layer and reach the PET filter regardless of the details of the following filtration of the suspension of nanotubes (Figure 4A−C), implying that this barrier of adjuvant powder is efficient against spurious adsorption of the nanotubes on the PET filter. However, one should be aware that this efficiency depends on the powder size, since an increased number of nanotubes were observed on the filter beneath the barrier cake when large crystal particles such as fructose were not milled into finer particles (Figure S7). In our collection procedure, fine powders of a size in the 10 μm range (insets of Figure 4A−C) were found to lead to optimal results.

The second step of the collection procedure, namely, the filtration of the suspension of nanotubes mixed with the adjuvant powder, creates a mixed adjuvant/nanotube layer over the bottom adjuvant barrier, which can be rinsed safely by successive washing/filtration steps with pure CH_2Cl_2 to eliminate residual PC. Next, the cake is collected and dissolved in water, leading to a suspension of nanotubes in water. If needed, for example for imaging purposes and evaluation of the collection procedure, these tubes can be collected by simple filtration over a PET membrane (Figure 4D−I).

We found that the intimate mixing of nanotubes and adjuvant powder in the second step of the collection procedure is required to avoid the formation of aggregates of nanotubes. Indeed, the simple filtration of the nanotube suspension over the previously prepared adjuvant cake, without adding adjuvant in the nanotube suspension, led to the formation of clusters of nanotubes (Figure S8), which could not be separated in water upon dissolution of the cake. In many cases, a large clump of aggregated nanotubes was even visible to the naked eye in the aqueous solution; therefore, the amount of nanotubes collected from the aqueous suspension was limited (Figure 4D), most of them being aggregated in this clump. In contrast, Figure 4E and F show that a much larger amount of free nanotubes are collected (compared to the case of Figure 4D) when using the complete collection route of Scheme 2. In addition, no trace of aggregated nanotubes was visible in the aqueous nanotube

DOI: 10.1021/acs.biomac.5b00628
Biomacromolecules XXXX, XXX, XXX−XXX

suspension with this collection strategy. This demonstrates that almost all nanotubes are trapped within the reservoir cake, and can be well dispersed in water during cake dissolution.

Although efficient, the method apparently leads to broken and deformed nanotubes losing their tubular shape (Figure 4G−I), with only a limited number of fully intact nanotubes when NaCl is used (Figure 4G); however, nanotubes collected using fructose and dextran are less affected by the collection (Figure 4H,I). In contrast, the nanotubes mostly retain their tubular shape just after dissolution of the PC templates in CH_2Cl_2 (Figures 2 and 3), indicating that deformation and fracture occur during at least one of the steps of our collection procedure in water. These steps involve (local) changes of ionic strength, generate concentration gradients and mechanical forces, and some of them could be detrimental to the integrity of the morphology of the nanotubes.

We suspected that the collection step for imaging purposes of the nanotubes from their aqueous dispersion was the main cause of nanotube damage, because filtration required the application of a significant force. Therefore, in order to observe more directly the nanotubes floating in the aqueous solution, Au/Cr-coated PET membranes and TEM carbon-coated grids were simply immersed in the aqueous dispersion of free nanotubes. The nanotubes adsorbed on these surfaces, allowing us to observe many intact cylindrical nanostructures (Figures 5 and 6), different from the deformed ones obtained after filtration (Figure 4G−I). Despite the fact that a few fragments still exist with this gentler collection method, it is obvious that the morphology of the nanotubes after filtration from an aqueous suspension does not reflect the one of nanotubes in the aqueous suspension; nanotubes in water essentially preserve their integrity.

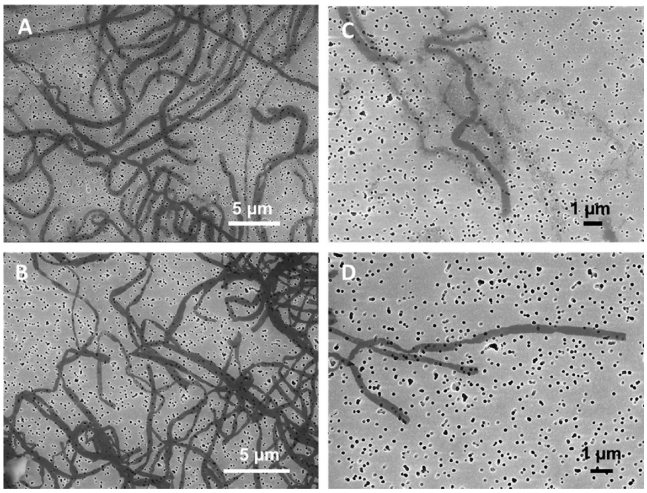

Figure 5. Images of nanotubes collected by adsorption on an Au/Cr-covered PET membrane from a dispersion in water obtained by the NaCl (A, C) and dextran (B, D)-aided collection method. The nanotube morphology is preserved by this gentler collection route.

Our hybrid nanotubes are certainly soft and swollen in water, being therefore prone to bending or fracture, especially because of their large aspect ratio (ca. 80 in this work). From our images, the maximum length was estimated to be 25 μm, while the external diameter of nanotubes depends on the adjuvant used (Figure 6D−F); when using NaCl, it is about 700 nm, twice the value found when fructose and dextran were used (ca. 350 nm). Moreover, the nanotubes collected with NaCl as adjuvant are porous (Figure 6D), which we attribute to salt-induced degradation resulting from the screening of electrostatic interactions between the polyelectrolytes in the NaCl-rich aqueous solution obtained after dissolution of the adjuvant; this hypothesis is also supported by the observation of enzyme release during collection (results shown later). More robust nanotubes are obtained when fructose and dextran are exploited as adjuvants (Figure 6E,F). In these cases, no significant morphological differences were found between nanotubes collected from CH_2Cl_2 and from water, except for the higher flexibility of water-collected nanotubes. As a conclusion, the extraction of nanotubes from polymer templates in a quantitative amount, followed by dispersion in water, was successfully achieved by the collection methodology of Scheme 2, yielding a clear aqueous dispersion of intact nanotubes when fructose or dextran is used as filtration adjuvant. It is noteworthy that this approach can also be applied to a variety of nanotubes or nanorods, as was reported elsewhere.[48]

Quantification of the Amount of Proteins in the Nanotubes. Attenuated total internal reflectance infrared spectroscopy (ATR-FTIR) is well established for probing in situ the internal structure of flat LbL films,[49−51] including water content, adsorbed mass of polyelectrolyte layers, ion pairing, and ratio between anionic and cationic monomer units. In contrast to planar films, the LbL growth of nanotubes occurs over the inner walls of nanopores within membranes, leading to the impracticability of conventional monitoring technologies commonly used for flat films, such as ATR-FTIR, quartz crystal microbalance (QCM),[52,53] or surface plasmon resonance (SPR).[54] So far, the growth of LbL films in cylindrical pores of PC membranes was quantified merely with respect to the variations of layer thickness,[55,56] with multilayers grown in confined spaces being generally thicker than those fabricated on an "open" planar surface under identical conditions. However, few report the internal composition of LbL films assembled in confinement.[57]

Herein, the nanotube wall composition was studied by FTIR measurements in transmission mode, after extraction of the nanotubes from the PC membranes (Figure 7). For GOX, the characteristic amide bands were observed in the 1410−1780 cm^{-1} range (two strong peaks at 1654 and 1541 cm^{-1}), as well as a C−H vibration at 1453 cm^{-1} (Figures 7 and S2). For bPEI, peaks at 1596 cm^{-1} (N−H bending vibration) and 1456 cm^{-1} (C−H stretching vibration) were prominent (Figures 7 and S2). For nanotubes, a weaker but apparent peak was also observed at 1773 cm^{-1}, corresponding to the O═C−O stretching vibration; this band was absent in the spectra of bPEI/GOX mixtures and was ascribed to residual traces of PC in the nanotube/KBr pellets. The protein amide I and amide II bands are very sensitive to any change of the protein secondary structure, which is important for enzymatic activity.[58] Comparing the IR spectra of free GOX and enzyme nanotubes, specifically the amide I and II bands at about 1654 and 1541 cm^{-1} (Figure 7), no significant difference was found, suggesting that the GOX component preserves its native secondary structure after complexation with bPEI in the nanotubes, a prerequisite for the preservation of its enzymatic activity.

The ratio by weight of bPEI to GOX in the nanotubes was obtained from a fit of the IR spectra, as detailed in the Experimental Section. As shown in Figures S2 and S4, the fitting curves matched the experimental IR data very well except for one- and two-bilayer nanotubes. The results of the fits are

DOI: 10.1021/acs.biomac.5b00628
Biomacromolecules XXXX, XXX, XXX−XXX

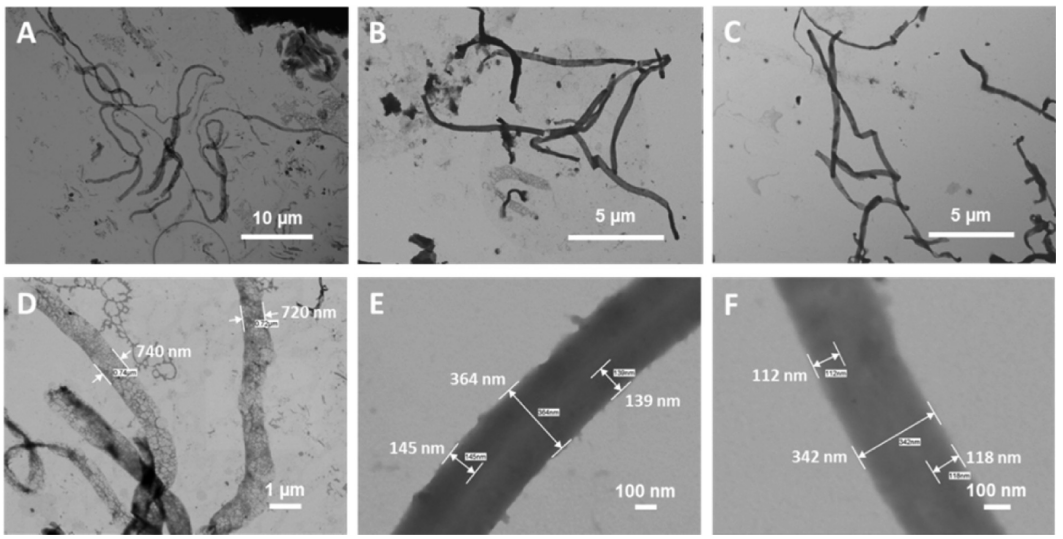

Figure 6. STEM images of nanotubes collected by adsorption on a TEM grid from a dispersion obtained by the adjuvant-aided collection method, with NaCl (A, D), fructose (B, E), and dextran (C, F) as adjuvants.

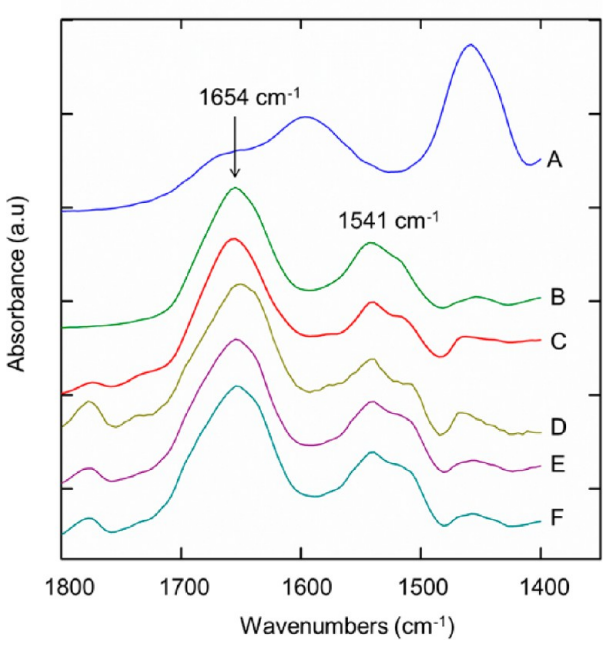

Figure 7. FTIR spectra of pure bPEI (A), GOX (B), $(bPEI/GOX)_6$ nanotubes (C), and undissolved clusters of nanotubes (six bilayers) collected from aqueous NaCl (D), fructose (E), or dextran (F) solutions, respectively. The spectra are shifted vertically for clarity. For the collection of the clusters, the nanotube suspension in CH_2Cl_2 was simply filtered over the adjuvant cake barrier, without adjuvant added to the CH_2Cl_2 suspension. After dissolution of the adjuvant cake in water, nanotube clusters were visible to the naked eye; they were picked up, rinsed in pure water, and then dried for FTIR measurements.

collected in Table S2, from which the proportion between the enzyme and bPEI was obtained for various numbers of bilayers. The bPEI/GOX weight ratio was almost constant at about 0.20 from 4 to 9 bilayers (for smaller numbers of bilayers, the signal was dominated by the traces of PC). The slight differences between samples is most likely due to the limited precision of the FTIR method for GOX-rich systems (as is the case here), to slight variations in the protocol, and possible evolution of the enzyme. These experiments show that GOX is largely dominating in the nanotubes, with an estimated weight fraction of about 80%, and that there is little variation depending on the number of bilayers. The large content in GOX of the nanotubes is evident from Figure 7, which shows almost identical spectra for the nanotubes and pure GOX. By knowing the weight fraction of GOX in the nanotubes, the ratio of the number of repeating units of bPEI ($-CH_2CH_2NH-$) per GOX macromolecule was calculated to be about 750.

Enzymatic Activity of Membrane-Immobilized and Liberated Nanotubes. Since the relative composition in GOX is about constant in the nanotubes, independent of the number of bilayers, the total amount of enzyme contained in the nanotubes simply scales linearly with the deposited volume V of the film, which can be directly obtained from the measured pore diameters R according to $V = \pi L(R_m^2 - R^2)$, where R_m is the radius of the bare pore and L is its length. Figure 8 shows that the pore diameter decreases regularly with the number of deposition cycles until eight bilayers, then saturates; in parallel, the nanotube wall thickness regularly increases then saturates. The volume deposited in the pore is also displayed in Figure 8; within experimental precision, the adsorbed volume and therefore the amount of incorporated enzyme, increases linearly with the number of cycles until it saturates above eight cycles.

The growth mechanism of polyelectrolytes in nanoporous templates was discussed extensively for the case of simple immersion in a previous article.[40] Two regimes exist in the evolution of wall thickness with number of deposition cycles, with a transition between the regimes for pores filled by about 70% (in the dry state). Below this threshold, the growth occurs as in flat films, with however quantitative differences in the amount of polyelectrolyte deposited per cycle. In the second regime when the pores are filled by more than about 70% (in the dry state), the pores are actually completely filled in solution due to multilayer swelling. Therefore, freshly brought polyelectrolytes only slowly diffuse in the highly hydrated filled nanopores, resulting in the formation of a progressively denser gel, and in a much slower relative increase of the dried wall thickness of nanotubes. In our case, 70% filling in the dried state corresponds to the transition from 8 to 9 bilayers, which explains why the growth of the LbL is slowed down at this

DOI: 10.1021/acs.biomac.5b00628
Biomacromolecules XXXX, XXX, XXX−XXX

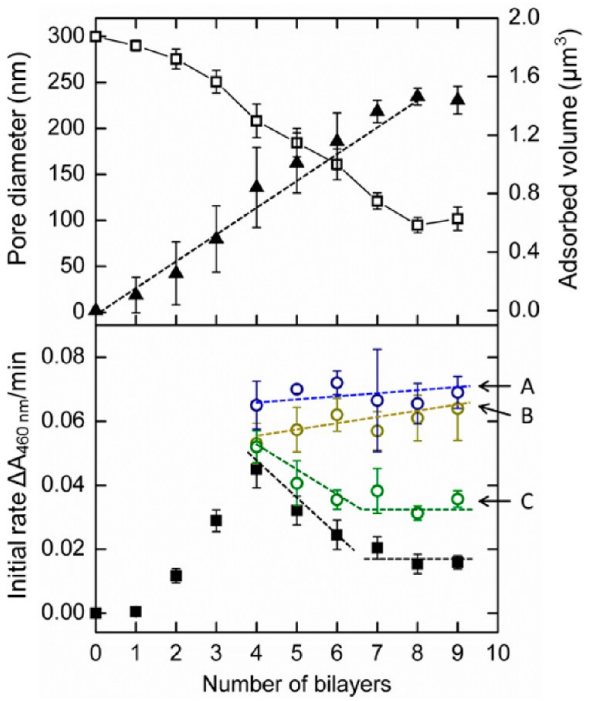

Figure 8. Pore diameter of LbL-filled membranes (open squares, left axis), adsorbed volume per pore (solid triangles, right axis), and activity of embedded (black squares) and freed (open circles) nanotubes as a function of the number of bilayers. The free nanotubes were collected with fructose (blue, A), NaCl (yellow, B), and dextran (green, C) as adjuvant during the collection. GOX in 10 mM HEPES buffer (pH 7.0) was alternately assembled with bPEI in 10 mM HEPES buffer (pH 7.0), followed by rinsing with the same buffer. The nanotube suspension was obtained by the adjuvant-aided collection method following Scheme 2, except for samples collected by using NaCl, in which case no NaCl was added to nanotube suspension in PC/CH_2Cl_2 in the second step of collection. The dotted lines are drawn to guide the eye.

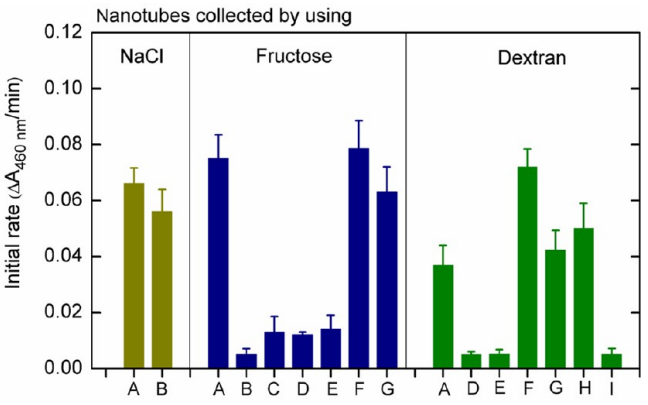

Figure 9. Activity of six-bilayer nanotube suspensions (columns A) obtained by using NaCl, fructose, and dextran as adjuvant, respectively, following the procedure of Scheme 2 (dissolution times were 5 min for NaCl and fructose and 45 min for dextran); activity of solutions after removal by filtration of the nanotubes from the relevant suspensions shown in columns A, after agitation of the aqueous nanotube suspensions for 5 min (columns B), 20 min (columns C), 1 h (columns D), and 2 h (columns E). Columns F and G show the activities of the six-bilayer nanotube aqueous suspensions, followed by (columns F) addition of 45 mg NaCl and 20 or 45 min gentle stirring for fructose- or dextran-based collected samples, respectively, and (columns G) removal of the nanotubes from this salted solution by filtration. Columns H and I follow the same protocols as columns F and G (dextran), respectively, except that 45 mg fructose was added instead of NaCl.

stage. In this growth regime, polyelectrolyte diffusion into the nanopores filled with the swollen multilayer becomes the limiting factor.

Although the amount of enzyme in the nanotubes increases close to linearly up to eight bilayers, the enzymatic activity of membrane-embedded nanotubes exhibits a maximum for four bilayers (Figure 8, full squares). Below this maximum, the activity logically increases with the number of bilayers due to the incorporation of larger amounts of enzyme; above this maximum, the activity decreases due to the restricted diffusion of the substrate into the increasingly narrower open channels of the tubes. Above eight bilayers, when the pores are fully filled by the swollen multilayers, the activity remains constant, corresponding to the limited variation of enzyme content in this regime and almost constant diffusion hindrances.

For activity measurements of liberated nanotubes, the role of the adjuvant used during the collection process was investigated in details. The use of NaCl as adjuvant results in a strong release of the enzyme from the nanotubes, due to the partial disassembly of the tubes in the presence of the relatively high ionic strength resulting from the dissolution of the adjuvant (Figure 9). The activity of an aqueous suspension of nanotubes was measured just after the dissolution of the adjuvant cake (A in Figure 9); then, intact nanotubes were removed by filtration after 5 min of gentle stirring, and the activity of the nanotube-free solution was measured again (B in Figure 9). For the NaCl adjuvant, the activity of the nanotube-free solution was high and identical to the initial one, demonstrating that the enzymes are not contained in the nanotubes: they are essentially present as free enzymes, or are complexed in very tiny fragments of tubes which are not filtered out. In contrast, when collected with fructose or dextran as adjuvants, the activity of filtered suspensions of nanotubes was much lower than prior to the removal of the nanotubes (Figure 9, compare columns A and B), even after 2 h agitation of the nanotube suspension (columns E), demonstrating that these adjuvants essentially do not release the enzyme from the tubes. These conclusions were fully confirmed by monitoring the activity of nanotubes still embedded in the membranes, after exposure to aqueous solutions containing 22.5 mg/mL of added NaCl, fructose, or dextran (Figure S9): while the addition of NaCl released a large amount of enzymes, no release was observed from the membranes exposed to fructose or dextran.

Nevertheless, significant differences are observed between the dextran and fructose-based collection methods, with a significantly smaller activity of the nanotubes observed when dextran is used as adjuvant (Figure 9, columns A). To check that these differences are not due to variations in the number of collected nanotubes, we added NaCl to the aqueous nanotube suspensions after their collection, in order to partially destroy the tubes and release as much as possible the GOX enzyme; the activity of these suspensions was then found to be nearly identical for the two adjuvants (Figure 9, columns F), suggesting that the amount of enzyme is indeed similar for the nanotubes collected in the presence of fructose or dextran. In addition, we monitored the activity of the free enzyme toward glucose in the presence of fructose or dextran and found no influence of the adjuvant (Figure S10); furthermore, no activity was exhibited by free GOX enzymes in the absence of

DOI: 10.1021/acs.biomac.5b00628
Biomacromolecules XXXX, XXX, XXX−XXX

glucose and in the presence of fructose or dextran (Figure S10). This confirms the highly specific catalytic activity of GOX toward its substance, D-glucose, and the absence of synergetic effects with fructose or dextran.

We also tested the catalytic activity toward glucose of planar $(GOX/bPEI)_{6.5}$ films in the presence and absence of adjuvant, in order to check whether the diffusion of the adjuvant into the LbL films modifies or not the film permeability toward glucose (Figure S11). Similarly to the free GOX enzyme, the activity of the 6.5-bilayer planar films toward glucose was found to be constant at about 0.015 min^{-1}, independent of the added fructose concentration, and identical to the one measured in the absence of fructose. However, the presence of dextran reduced slightly the activity to about 0.013 min^{-1}. This small variation suggests that dextran might slightly impede the diffusion of glucose in the films, maybe due to limited adsorption on the surface. At any rate, this effect is minor and cannot explain the large difference of activity between nanotubes collected in the presence of fructose or dextran (about a factor of 2 as shown in Figure 9), since no dextran was detected on/within nanotubes by FTIR spectroscopy (Figure S12).

The main difference between fructose and dextran is their molar mass, and therefore, the associated difference of osmotic pressure resulting from the difference of concentration of the adjuvant in the aqueous solution and in the nanotube. As a result, much larger swelling forces are exerted on the nanotubes when in the presence of fructose, which might very well explain the subsequent increased permeability of the nanotubes toward glucose. An experiment was performed to support this hypothesis: The nanotubes were collected with either fructose or dextran as adjuvant, then NaCl was added to the suspensions to disrupt the nanotubes. The suspensions were then filtered to remove intact nanotubes, and the residual activity of the nanotube-free solutions were measured again (columns G in Figure 9). The residual activity was significantly larger for the fructose collection route compared to the dextran-based one, indicating that the nanotubes were much less resistant to NaCl in the presence of fructose than in the presence of dextran. Furthermore, the addition of fructose in the nanotube suspension obtained with dextran as adjuvant increases moderately the activity (column H in Figure 9), although this effect is weaker than when adding NaCl. These observations support the notion that fructose swells more strongly the nanotubes than dextran and contributes to their disruption. Therefore, we also associate the larger activity of the nanotubes in the presence of fructose to their higher degree of swelling and therefore easier accessibility of glucose to the enzymes. In contrast, the accessibility of glucose to the enzyme in dextran-collected nanotubes is hindered to some extent by their lower degree of swelling. Therefore, in the sequel, we concentrate on the dextran-based route, as it is more innocuous to the structure of the nanotubes.

As was evidenced, the amount of enzyme incorporated in the nanotubes increases linearly with LbL growth, until saturation is reached for eight bilayers. This is not the case for the activity, shown in Figure 8 for the membrane-embedded nanotubes, the dextran-collected free nanotubes, fructose-collected free nanotubes, and the NaCl-collected free (and largely destroyed) nanotubes. No significant difference of activity is seen for these three systems for four bilayers; below this number, free intact tubes could not be collected due to their too weak mechanical properties. However, the activity of membrane-embedded nanotubes simply scales linearly below four bilayers, and it is most likely also the case of the free nanotubes. Above four bilayers, the nanotubes collected with NaCl and fructose as adjuvant exhibit a much larger activity than membrane-embedded nanotubes, due to the massive release of the enzyme for NaCl-collected nanotubes and the higher swelling of fructose-collected nanotubes in this collection condition.

In contrast, liberated nanotubes collected in the presence of dextran exhibit an activity which follows a similar trend as nanotubes embedded in the membrane, although their activity is significantly higher. Contrarily to nanotubes embedded in the templates, the free dextran/fructose-collected nanotubes have no limitation of accessibility around their outer surfaces, thereby enabling the diffusion of glucose and products in and out of nanotubes not only from their ends and inner surface but also through their hydrated external walls as reported elsewhere.[15] It is significant that the observed difference of activity of membrane-embedded and dextran-collected free nanotubes is about a factor of 2 (in the plateau region), which corresponds roughly to the increase of the accessible surface for free nanotubes compared to embedded ones.

CONCLUSIONS

Robust glucose oxidase-loaded nanotubes were synthesized by template-assisted layer-by-layer assembly. A quantitative collection methodology was developed based on adjuvant-assisted filtration, with either NaCl, fructose, or dextran as adjuvant. While NaCl induces a release of enzymes from liberated nanotubes, clear aqueous suspensions of nanotubes of intact tubular morphology could be obtained with fructose or dextran. Nevertheless, the larger osmotic pressure of fructose compared to dextran leads to less stable and more swollen nanotubes; as a consequence, the use of dextran is recommended, leading to the efficient and quantitative extraction of nanotubes from the membrane templates. FTIR results showed that the enzyme dominates the nanotubes by weight, with a content of about 80% independent of the number of bilayers, and that the enzyme retains its protein secondary structure in the nanotubes, indicating that the enzyme survives the collection process. The enzymatic activity of the nanotubes either embedded in the membrane or released in suspension was measured. The activity of embedded nanotubes exhibits a maximum for four bilayers due to the interplay between the amount of enzyme embedded in the tubes and the accessibility of glucose to the enzyme; dextran-collected freed nanotubes display a similar trend, but have a higher activity than embedded nanotubes thanks to the increased diffusion of the enzyme substrate through external lateral surfaces. As for fructose-collected free nanotubes, they exhibit an even higher activity most probably due to very swollen walls of the nanotubes. These nanotubular enzymatic structures thus appear as promising swarming agents for the transformation of glucose in a solution; the generalization of this approach to other enzymes would broaden even further perspectives of application.

ASSOCIATED CONTENT

Supporting Information

SEM image of the membrane before and after LbL templating, and STEM images showing the tubular structure of the nanotubes (Figures S1a and S1b); sample preparation for STEM using the ice immobilization route (Scheme S1); details on the FTIR fitting procedure including the establishment of

DOI: 10.1021/acs.biomac.5b00628
Biomacromolecules XXXX, XXX, XXX−XXX

the calibration curve (Figures S2−S3, Table S1), fitting results (Figure S4 and Table S2), and FTIR spectra of pure KBr and polycarbonate (Figure S5); STEM image of a thin film of nanotubes prepared using the ice collection route (Figure S6); SEM images related to the collection of nanotubes with fructose of large grain size (Figure S7) and in the absence of adjuvant added to the nanotube suspension (Figure S8); effect of adjuvants on the stability of 6-bilayer nanotubes embedded inside templates (Figure S9), on the activity of free GOX toward glucose (Figure S10), and on the activity of a flat $(GOX/bPEI)_{6.5}$ film (Figure S11); and FTIR spectra of pure dextran and liberated tubes collected from dextran solution (Figure S12). The Supporting Information is available free of charge on the ACS Publications website at DOI: 10.1021/acs.biomac.5b00628.

AUTHOR INFORMATION

Corresponding Authors

*E-mail: sophie.demoustier@uclouvain.be.
*E-mail: alain.jonas@uclouvain.be.

Notes

The authors declare no competing financial interest.

ACKNOWLEDGMENTS

We are grateful to Etienne Ferain and the it4ip company for supplying the nanoporous PC and PET membranes, Delphine Magnin, Colette Douchamps, and Pascale Lipnik for assistance with SEM and STEM measurements and materials, and Diana Ramirez-Wong, Saghi Saghazadeh, and Alina Osypova for helpful discussions on LbL assembly. S.Z. acknowledges a Ph.D. scholarship from the China Scholarship Council (CSC). The work was supported financially by the Belgian Federal Science Policy (IAP program P7/05).

REFERENCES

(1) Chiu, D. T.; Wilson, C. F.; Ryttsen, F.; Stromberg, A.; Farre, C.; Karlsson, A.; Nordholm, S.; Gaggar, A.; Modi, B. P.; Moscho, A.; Garza-Lopez, R. A.; Orwar, O.; Zare, R. N. Chemical transformations in individual ultrasmall biomimetic containers. *Science* **1999**, *283*, 1892−1895.

(2) Inokuma, Y.; Kawano, M.; Fujita, M. Crystalline molecular flasks. *Nat. Chem.* **2011**, *3*, 349−358.

(3) Vriezema, D. M.; Comellas Aragones, M.; Elemans, J. A.; Cornelissen, J. J.; Rowan, A. E.; Nolte, R. J. Self-assembled nanoreactors. *Chem. Rev.* **2005**, *105*, 1445−1489.

(4) Koblenz, T. S.; Wassenaar, J.; Reek, J. N. Reactivity within a confined self-assembled nanospace. *Chem. Soc. Rev.* **2008**, *37*, 247−262.

(5) Zeng, T.; Zhang, X.; Wang, S.; Ma, Y.; Niu, H.; Cai, Y. Assembly of a nanoreactor system with confined magnetite core and shell for enhanced Fenton-like catalysis. *Chem. - Eur. J.* **2014**, *20*, 6474−6481.

(6) Vriezema, D. M.; Garcia, P. M.; Sancho Oltra, N.; Hatzakis, N. S.; Kuiper, S. M.; Nolte, R. J.; Rowan, A. E.; van Hest, J. C. Positional assembly of enzymes in polymersome nanoreactors for cascade reactions. *Angew. Chem., Int. Ed.* **2007**, *46*, 7378−7382.

(7) Bolinger, P. Y.; Stamou, D.; Vogel, H. An integrated self-assembled nanofluidic system for controlled biological chemistries. *Angew. Chem., Int. Ed.* **2008**, *47*, 5544−5549.

(8) Ghan, R.; Shutava, T.; Patel, A.; John, V. T.; Lvov, Y. Enzyme-Catalyzed Polymerization of Phenols within Polyelectrolyte Microcapsules. *Macromolecules* **2004**, *37*, 4519−4524.

(9) Caruso, F.; Schüler, C. Enzyme Multilayers on Colloid Particles: Assembly, Stability, and Enzymatic Activity. *Langmuir* **2000**, *16*, 9595−9603.

(10) del Mercato, L. L.; Carraro, M.; Zizzari, A.; Bianco, M.; Miglietta, R.; Arima, V.; Viola, I.; Nobile, C.; Soraru, A.; Vilona, D.; Gigli, G.; Bonchio, M.; Rinaldi, R. Catalytic self-propulsion of supramolecular capsules powered by polyoxometalate cargos. *Chem. - Eur. J.* **2014**, *20*, 10910−10914.

(11) Orozco, J.; Garcia-Gradilla, V.; D'Agostino, M.; Gao, W.; Cortes, A.; Wang, J. Artificial enzyme-powered microfish for water-quality testing. *ACS Nano* **2013**, *7*, 818−824.

(12) Komatsu, T.; Sato, T.; Boettcher, C. Human serum albumin nanotubes with esterase activity. *Chem. - Asian J.* **2012**, *7*, 201−206.

(13) Yu, A.; Liang, Z.; Caruso, F. Enzyme Multilayer-Modified Porous Membranes as Biocatalysts. *Chem. Mater.* **2005**, *17*, 171−175.

(14) Komatsu, T.; Terada, H.; Kobayashi, N. Protein nanotubes with an enzyme interior surface. *Chem. - Eur. J.* **2011**, *17*, 1849−1854.

(15) Hou, S.; Wang, J.; Martin, C. R. Template-synthesized protein nanotubes. *Nano Lett.* **2005**, *5*, 231−234.

(16) Fakhrullin, R. F.; Paunov, V. N. Fabrication of living cellosomes of rod-like and rhombohedral morphologies based on magnetically responsive templates. *Chem. Commun.* **2009**, 2511−2513.

(17) Hou, S.; Wang, J.; Martin, C. R. Template-synthesized DNA nanotubes. *J. Am. Chem. Soc.* **2005**, *127*, 8586−8587.

(18) Hou, S.; Harrell, C. C.; Trofin, L.; Kohli, P.; Martin, C. R. Layer-by-layer nanotube template synthesis. *J. Am. Chem. Soc.* **2004**, *126*, 5674−5675.

(19) He, Q.; Cui, Y.; Ai, S.; Tian, Y.; Li, J. Self-assembly of composite nanotubes and their applications. *Curr. Opin. Colloid Interface Sci.* **2009**, *14*, 115−125.

(20) Komatsu, T. Protein-based nanotubes for biomedical applications. *Nanoscale* **2012**, *4*, 1910−1918.

(21) Perry, J. L.; Martin, C. R.; Stewart, J. D. Drug-delivery strategies by using template-synthesized nanotubes. *Chem. - Eur. J.* **2011**, *17*, 6296−6202.

(22) Kim, J.; Yoo, K. H. Glucose oxidase nanotube-based enzymatic biofuel cells with improved laccase biocathodes. *Phys. Chem. Chem. Phys.* **2013**, *15*, 3510−3517.

(23) Decher, G. Fuzzy Nanoassemblies: Toward Layered Polymeric Multicomposites. *Science* **1997**, *277*, 1232−1237.

(24) Landoulsi, J.; Roy, C. J.; Dupont-Gillain, C.; Demoustier-Champagne, S. Synthesis of collagen nanotubes with highly regular dimensions through membrane-templated layer-by-layer assembly. *Biomacromolecules* **2009**, *10*, 1021−1024.

(25) Landoulsi, J.; Demoustier-Champagne, S.; Dupont-Gillain, C. Self-assembled multilayers based on native or denatured collagen: mechanism and synthesis of size-controlled nanotubes. *Soft Matter* **2011**, *7*, 3337−3347.

(26) Qu, X.; Lu, G.; Tsuchida, E.; Komatsu, T. Protein nanotubes comprised of an alternate layer-by-layer assembly using a polycation as an electrostatic glue. *Chem. - Eur. J.* **2008**, *14*, 10303−10308.

(27) Qu, X.; Komatsu, T. Molecular capture in protein nanotubes. *ACS Nano* **2010**, *4*, 563−573.

(28) Lu, G.; Tsuchida, E.; Komatsu, T. Human Serum Albumin Nanotubes Comprising Layer-by-layer Assembly with Polycation. *Chem. Lett.* **2008**, *37*, 972−973.

(29) Tian, Y.; He, Q.; Cui, Y.; Li, J. Fabrication of protein nanotubes based on layer-by-layer assembly. *Biomacromolecules* **2006**, *7*, 2539−2542.

(30) Dougherty, S. A.; Zhang, D.; Liang, J. Fabrication of protein nanotubes using template-assisted electrostatic layer-by-layer methods. *Langmuir* **2009**, *25*, 13232−13237.

(31) Lu, G.; Ai, S.; Li, J. Layer-by-layer assembly of human serum albumin and phospholipid nanotubes based on a template. *Langmuir* **2005**, *21*, 1679−1682.

(32) de la Escosura, A.; Nolte, R. J. M.; Cornelissen, J. J. L. M. Viruses and protein cages as nanocontainers and nanoreactors. *J. Mater. Chem.* **2009**, *19*, 2274−2278.

(33) Roy, C. J.; Buron, C. C.; Demoustier-Champagne, S.; Jonas, A. M. Nanoconfined Polyelectrolyte Multilayers From Nanostripes to Multisegmented Functional Nanotubes. In *Multilayer Thin Films: Sequential Assembly of Nanocomposite Materials*, 2nd ed.; Decher, G.,

DOI: 10.1021/acs.biomac.5b00628
Biomacromolecules XXXX, XXX, XXX−XXX

Schlenoff, J. B., Eds.; Wiley-VCH Verlag & Co. KGaA: Weinheim, Germany, 2012; pp 613−636.
(34) Pescador, P.; Katakis, I.; Toca-Herrera, J. L.; Donath, E. Efficiency of a bienzyme sequential reaction system immobilized on polyelectrolyte multilayer-coated colloids. *Langmuir* **2008**, *24*, 14108−14114.
(35) Lvov, Y.; Ariga, K.; Ichinose, I.; Kunitake, T. Assembly of Multicomponent Protein Films by Means of Electrostatic Layer-by-Layer Adsorption. *J. Am. Chem. Soc.* **1995**, *117*, 6117−6123.
(36) Onda, M.; Ariga, K.; Kunitake, T. Activity and stability of glucose oxidase in molecular films assembled alternately with polyions. *J. Biosci. Bioeng.* **1999**, *87*, 69−75.
(37) Schüler, C.; Caruso, F. Preparation of enzyme multilayers on colloids for biocatalysis. *Macromol. Rapid Commun.* **2000**, *21*, 750−753.
(38) Suh, J.; Paik, H. J.; Hwang, B. K. Ionization of Poly(ethylenimine) and Poly(allylamine) at Various pH's. *Bioorg. Chem.* **1994**, *22*, 318−327.
(39) Nagaya, J.; Homma, M.; Tanioka, A.; Minakata, A. Relationship between protonation and ion condensation for branched poly(ethylenimine). *Biophys. Chem.* **1996**, *60*, 45−51.
(40) Roy, C. J.; Dupont-Gillain, C.; Demoustier-Champagne, S.; Jonas, A. M.; Landoulsi, J. Growth mechanism of confined polyelectrolyte multilayers in nanoporous templates. *Langmuir* **2010**, *26*, 3350−3355.
(41) Bertrand, P.; Jonas, A.; Laschewsky, A.; Legras, R. Ultrathin polymer coatings by complexation of polyelectrolytes at interfaces: suitable materials, structure and properties. *Macromol. Rapid Commun.* **2000**, *21*, 319−348.
(42) Lourenco, J. M.; Ribeiro, P. A.; Botelho do Rego, A. M.; Raposo, M. Counterions in layer-by-layer films–influence of the drying process. *J. Colloid Interface Sci.* **2007**, *313*, 26−33.
(43) Qu, X.; Kobayashi, N.; Komatsu, T. Solid nanotubes comprising alpha-Fe2O3 nanoparticles prepared from ferritin protein. *ACS Nano* **2010**, *4*, 1732−1738.
(44) Chia, K. K.; Rubner, M. F.; Cohen, R. E. pH-responsive reversibly swellable nanotube arrays. *Langmuir* **2009**, *25*, 14044−14052.
(45) Yang, Y.; He, Q.; Duan, L.; Cui, Y.; Li, J. Assembled alginate/chitosan nanotubes for biological application. *Biomaterials* **2007**, *28*, 3083−3090.
(46) Ai, S.; He, Q.; Tao, C.; Zheng, S.; Li, J. Conductive Polypyrrole and Poly(allylamine hydrochloride) Nanotubes Fabricated with Layer-by-Layer Assembly. *Macromol. Rapid Commun.* **2005**, *26*, 1965−1969.
(47) Bieker, P.; Schönhoff, M. Linear and Exponential Growth Regimes of Multilayers of Weak Polyelectrolytes in Dependence on pH. *Macromolecules* **2010**, *43*, 5052−5059.
(48) Saghazadeh, S.; Zhang, S.; Lefevre, D.; Le Beulze, A.; Jonas, A. M.; Demoustier-Champagne, S. Universal Method to Transfer Membrane-Templated Nano-Objects to Aqueous Solutions. *Langmuir* **2015**, *31*, 1.
(49) Sukhishvili, S. A.; Granick, S. Layered, Erasable Polymer Multilayers Formed by Hydrogen-Bonded Sequential Self-Assembly. *Macromolecules* **2002**, *35*, 301−310.
(50) Boudou, T.; Crouzier, T.; Auzely-Velty, R.; Glinel, K.; Picart, C. Internal composition versus the mechanical properties of polyelectrolyte multilayer films: the influence of chemical cross-linking. *Langmuir* **2009**, *25*, 13809−13819.
(51) Crouzier, T.; Picart, C. Ion pairing and hydration in polyelectrolyte multilayer films containing polysaccharides. *Biomacromolecules* **2009**, *10*, 433−442.
(52) Lvov, Y.; Ariga, K.; Ichinose, I.; Kunitake, T. Molecular film assembly via layer-by-layer adsorption of oppositely charged macromolecules (linear polymer, protein and clay) and concanavalin A and glycogen. *Thin Solid Films* **1996**, *284−285*, 797−801.
(53) Lvov, Y. M.; Lu, Z.; Schenkman, J. B.; Zu, X.; Rusling, J. F. Direct Electrochemistry of Myoglobin and Cytochrome P450camin Alternate Layer-by-Layer Films with DNA and Other Polyions. *J. Am. Chem. Soc.* **1998**, *120*, 4073−4080.
(54) Mendelsohn, J. D.; Yang, S. Y.; Hiller, J.; Hochbaum, A. I.; Rubner, M. F. Rational design of cytophilic and cytophobic polyelectrolyte multilayer thin films. *Biomacromolecules* **2003**, *4*, 96−106.
(55) Lee, D.; Nolte, A. J.; Kunz, A. L.; Rubner, M. F.; Cohen, R. E. pH-induced hysteretic gating of track-etched polycarbonate membranes: swelling/deswelling behavior of polyelectrolyte multilayers in confined geometry. *J. Am. Chem. Soc.* **2006**, *128*, 8521−8529.
(56) Alem, H.; Blondeau, F.; Glinel, K.; Demoustier-Champagne, S.; Jonas, A. M. Layer-by-Layer Assembly of Polyelectrolytes in Nanopores. *Macromolecules* **2007**, *40*, 3366−3372.
(57) Ramírez-Wong, D. G.; Coelho-Diogo, C.; Aimé, C.; Bonhomme, C.; Jonas, A. M.; Demoustier-Champagne, S. Effects of geometrical confinement in membrane pores on enzyme-based layer-by-layer assemblies. *Appl. Surf. Sci.* **2015**, *338*, 154−162.
(58) Delfino, I.; Portaccio, M.; Ventura, B. D.; Mita, D. G.; Lepore, M. Enzyme distribution and secondary structure of sol−gel immobilized glucose oxidase by micro-attenuated total reflection FT-IR spectroscopy. *Mater. Sci. Eng., C* **2013**, *33*, 304−310.

DOI: 10.1021/acs.biomac.5b00628
Biomacromolecules XXXX, XXX, XXX−XXX